Supporting Information for

Etching- and Intermediate-free Graphene Dry Transfer onto Polymeric Thin Films with High Piezoresistive Gauge Factors

Runlai Li,*†[a] Qinghua Zhang,*[a] Eric Zhao,[b] Jin Li,[a] Qiao Gu[a] and Ping Gao†[a]

a. Department of Chemical and Biological Engineering, The Hong Kong University of Science and Technology, Clear Water Bay, Kowloon, Hong Kong SAR, PRC

b. Department of Chemical Engineering, Stanford University, Stanford, California 94305-5025, United States

* Equal contributors

†Co-corresponding Authors: Prof. Ping Gao, kepgao@ust.hk; Dr. Runlai Li, rliae@connect.ust.hk

1. Experimental

Materials

Ultra high molecular weight polyethylene (UHMWPE) resin (GUR 4022) with weight average molecular weight of 3.5 million Dalton was purchase from Celanese China Ltd. 25 micron-thick copper foils (No. 46365) were purchased from Alfa Aesar as catalyst metal layer for graphene growth in CVD.

Methods

Graphene synthesis

Monolayer graphene was fabricated using the standard chemical vapor deposition (CVD) method.[1] Briefly, copper foils loaded inside a ThermoFisher Lindberg/Blue MTM furnace with programmable temperature settings. Argon with purity >99.999% at 270 sccm, 40 psi was used to evacuate the tubular furnace for 5-mins at the ambient temperatures. The system is then heated up to 1000 ^{o}C at a ramping rate of 65 ^{o}C/min. Upon reaching 1000 ^{o}C, the system was held for 20 mins to reduce the copper surface and remove internal stresses in the as-received copper foil. Finally, the setup was further heated to 1050 ^{o}C for graphene deposition. During the entire heating and subsequent cooling processes, the flow of ultra-high purity hydrogen at 10 sccm and 40 psi together with the argon gas was maintained. In addition, a flow of 200 ppm CH4 at 90 sccm, 40 psi was introduced and maintained for 30 mins when the system reached 1050 ^{o}C. As soon as the CH4 flow was stopped, heating was switched off, and the graphene deposition section was rapidly cooled down by sliding off from the furnace.

UHMWPE thin film preparation

The 4-micron-thick porous UHMWPE films were prepared using a method similar to that was developed by Li and Gao for the fabrication of nanoporous UHMWPE safer separators for high-power-density rechargeable batteries.[2]

Scanning electron microscopy (SEM)

SEM micro-photos were captured with JEOL 7800, with an acceleration voltage of 5 kV and a working distance of 10.4 mm.

Energy-dispersive X-ray spectrometry (EDX)

X-Max^{N} silicon drift detector from Oxford Instruments was used to perform SEM in-situ EDX elemental mapping with an acceleration voltage of 10kV.

Atomic force microscopy (AFM)

Surface topography was characterized by Veeco multimode atomic force microscope. The scanning range can be up to 200 µm laterally and 10 µm vertically. Tapping mode measures topography by tapping the surface with oscillating tip, avoiding damage to gPE surfaces by shear forces. Bruker ScanAsyst-Air were used for scanning tips with a radius of 2 nm. The triangular cantilever is made by silicon nitride with a layer of reflective aluminum coating on the backside.

Micro-Raman spectroscopy and mapping

Lamination of graphene on UHMWPE thin film at the microscopic level was characterized using micro-Raman spectral mapping scanning on the micro-Raman spectrometer, (Renshaw InVia). Argon laser radiation of 514 nm and 0.10 mW through a 50x lens was used to minimize the surface heating effect. Scanning was performed from 3000 cm^{-1} to 1000 cm^{-1}, with a scanning speed of 200 cm^{-1}/sec.

Differential scanning calorimetry (DSC)

DSC was carried out on a TA Q1000 DSC, ramping from 0 to 180 °C at 20 °C/min. To simulate the thermal history of annealing with biaxial constraint force, films were folded and loaded between flat aluminum pans, then compressed together before DSC tests.

UV-vis Photospectroscopy

We conducted ultraviolet-Visible spectroscopy analysis on a Perkin Lambda 20 UV/VIS spectrometer. We employed incident irradiation emissions with wavelengths between 200 nm and 1100 nm and scanned the light transmittance through our samples at a standard scanning rate of 480 nm wavenumbers/min. Before each measurement, we calibrated the spectrometric transmission through the air as the reference for 100% transmittance.

2. Supplementary Results and Discussion

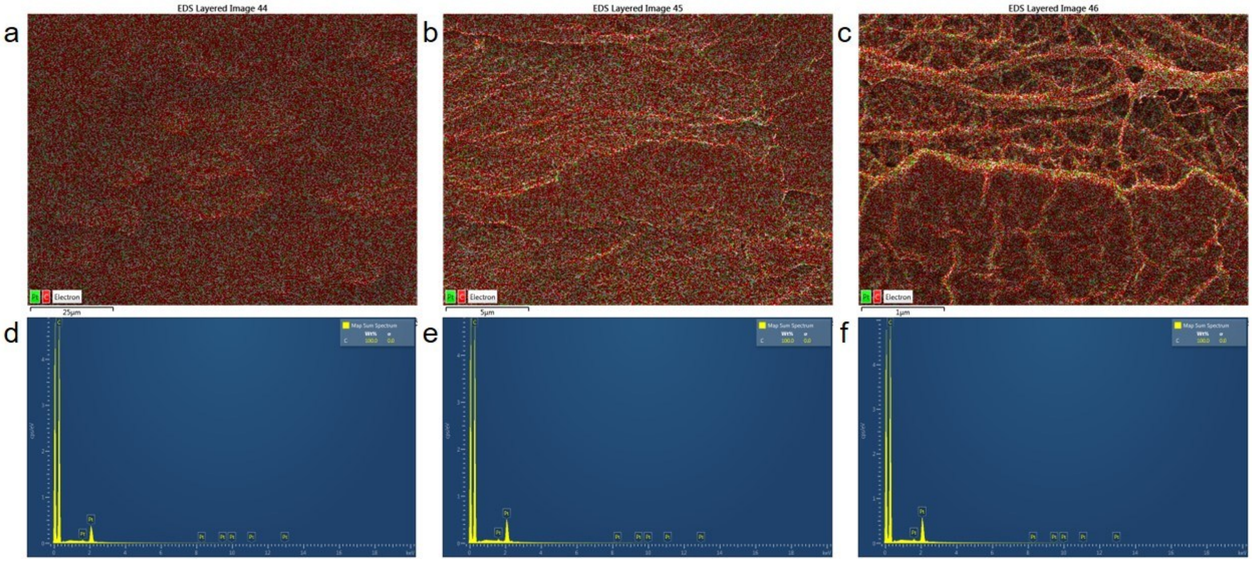

Fig. S1 In-situ energy-dispersive X-ray spectrometry installed in SEM of graphene/UHMWPE composite thin film. The measurements were performed at three different spots, and the mapping results are shown in (a-c), while the corresponding spectra are in (d-f).

In-situ EDX in SEM was performed to check any copper residue on gPE surface after the exfoliation transfer. No copper element was captured by EDX after scanning at three different locations on gPE, as shown in **Fig. S1**.

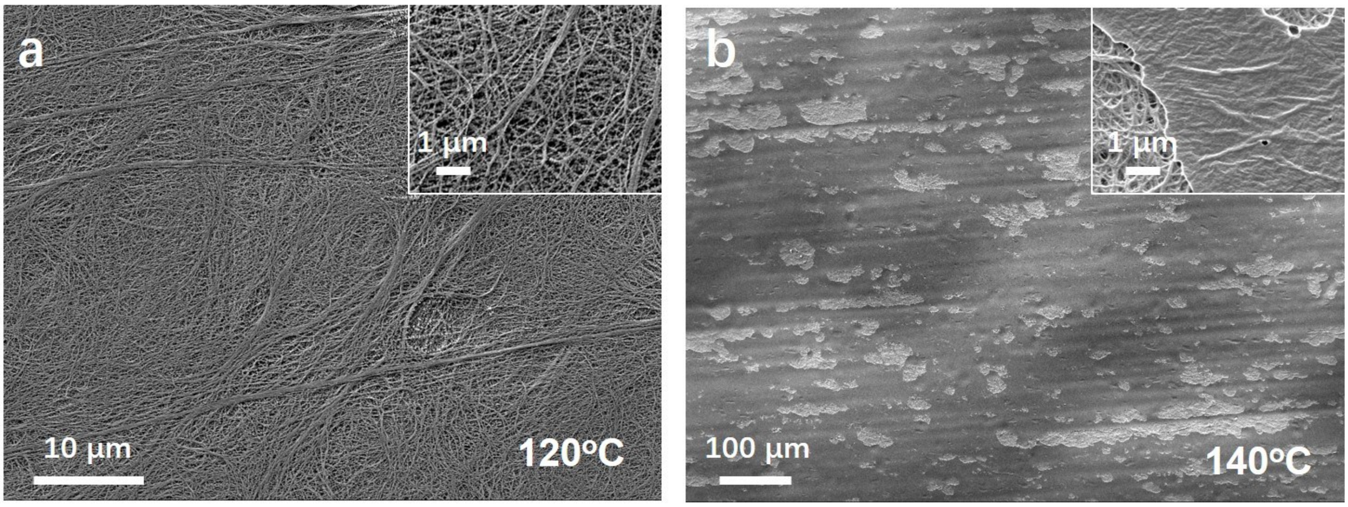

Fig. S2 Annealing temperature effect on the efficiency of graphene transfer. (a) Copper/graphene foil exfoliated after annealing at 120°C for 5 minutes. (b) Copper/graphene foil exfoliated after annealing at 120°C for 5 minutes.

The thermal annealing of the films at elevated temperatures ranged from 80°C to 180°C at 20°C intervals. The minimum temperature for effective graphene transfer was 140°C, which was close to the melting point of FCC of PE (141.2°C) characterized by DSC in **Fig. 4e**. These results further support that the selective melting between FCC and ECC of PE is the fundamental cause for the enhanced vdW interaction between PE and graphene.

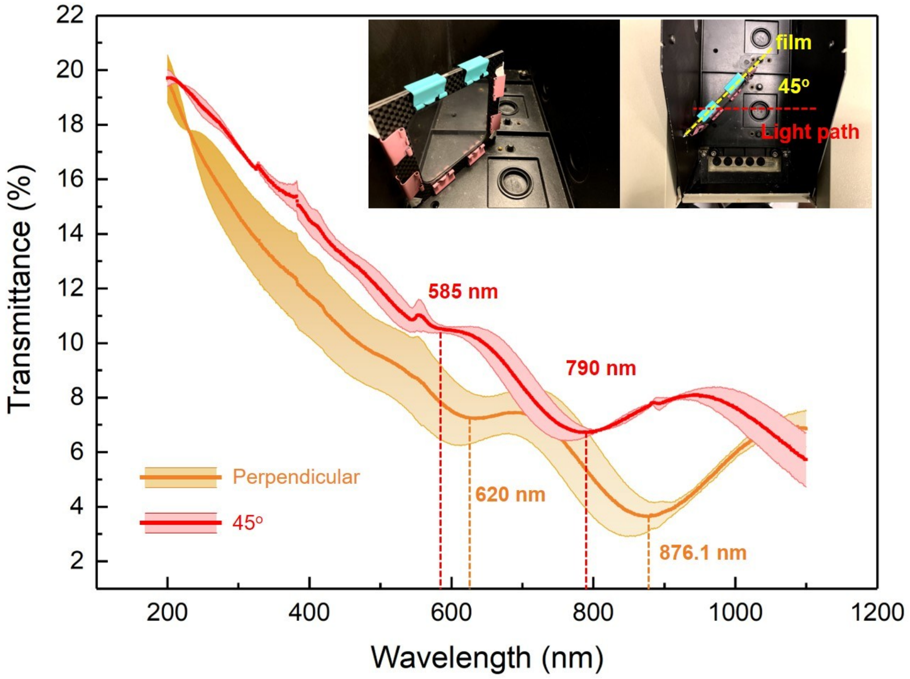

Fig. S3 UV-vis transmittance of PE after annealing changed by graphene lamination. The orange line represents the averaged result measured by loading the film perpendicular to the light path during the UV-vis test. While the red one represents the averaged result when the angle between sample and light path was 45°, as demonstrated by the two inserts. The measurements were repeated at the different spots all over the film for 8 times, and the bands stand for the error bands.

By tilting the film for 45°, the light path within the film will be increased and thus the specific wavelength for destructive interference occurring will be altered, as shown in Fig. S3. The phenomenon could be observed by naked eyes as demonstrated in Video S2.

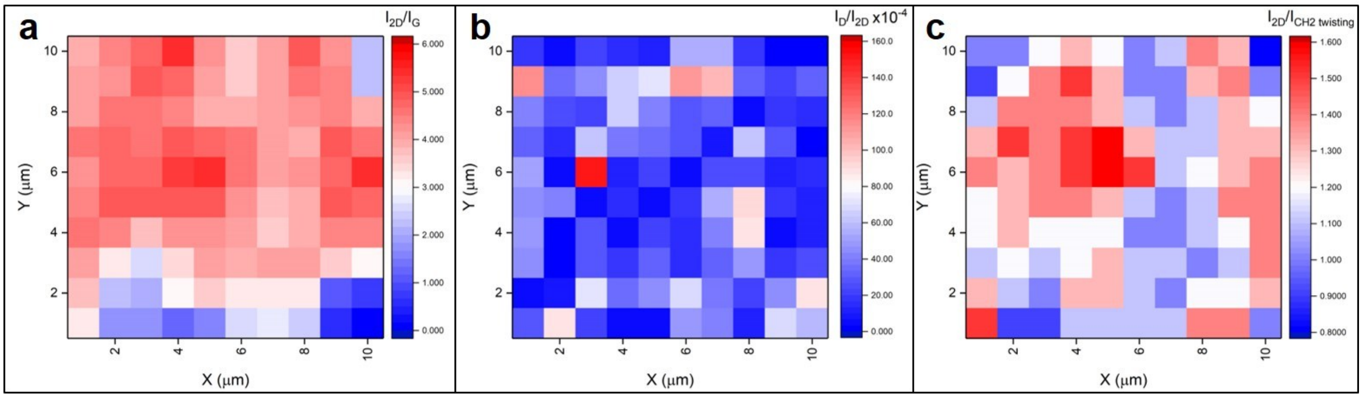

Fig. S4 Micro-Raman shift spectrum of gPE over 10 μm×10 μm with the resolution of 1 μm. (a-c) Micro-Raman intensity ratio heat map on I_{2D}/I_G, I_D/I_{2D} and $I_{2D}/I_{CH2.}$

The scanning area is at the of the mapping area presented in **Fig. 4**. These results proved that the high-quality, high transfer-efficiency and homogeneity of graphene on PE.

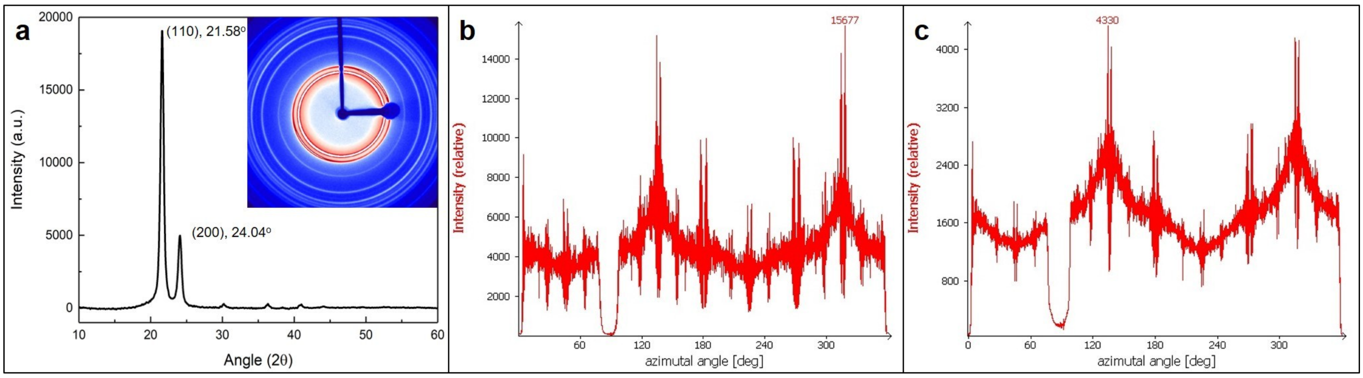

Fig. S5 XRD results of PE films. (a) Powder XRD result of PE, the insert shows the 2D WAXS pattern of PE. (b-c) the corresponding azimuthal-integrated intensity distribution of WAXS patterns of (110) and (200) planes.

Powder XRD and WAXS were performed to investigate the crystalline isotropy of PE, which proved that the prepared PE films were isotropic in 2D directions. The crystalline isotropy guarantees the homogeneity of mechanical properties of PE in 2D directions.

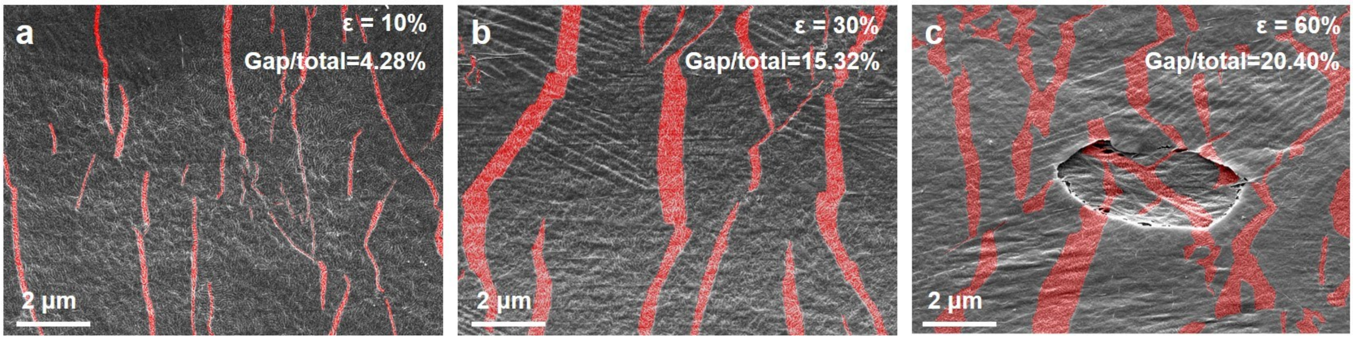

Fig. S6 SEM micro-phots of gPE surface morphologies after the elevated strain: (a) 10%, (b) 30%, and (c) 60%.

It could be observed that cracks developed broader and more emerged when strain increased. Some cracks extended into the pinholes as shown in **Fig. S6c**, proved that graphene was continuous. This result further proved that even in the pinhole, graphene could be effectively transferred. Quantitative analysis of graphene coverage in PE pinholes was conducted and the results were shown in **Fig. S7**.

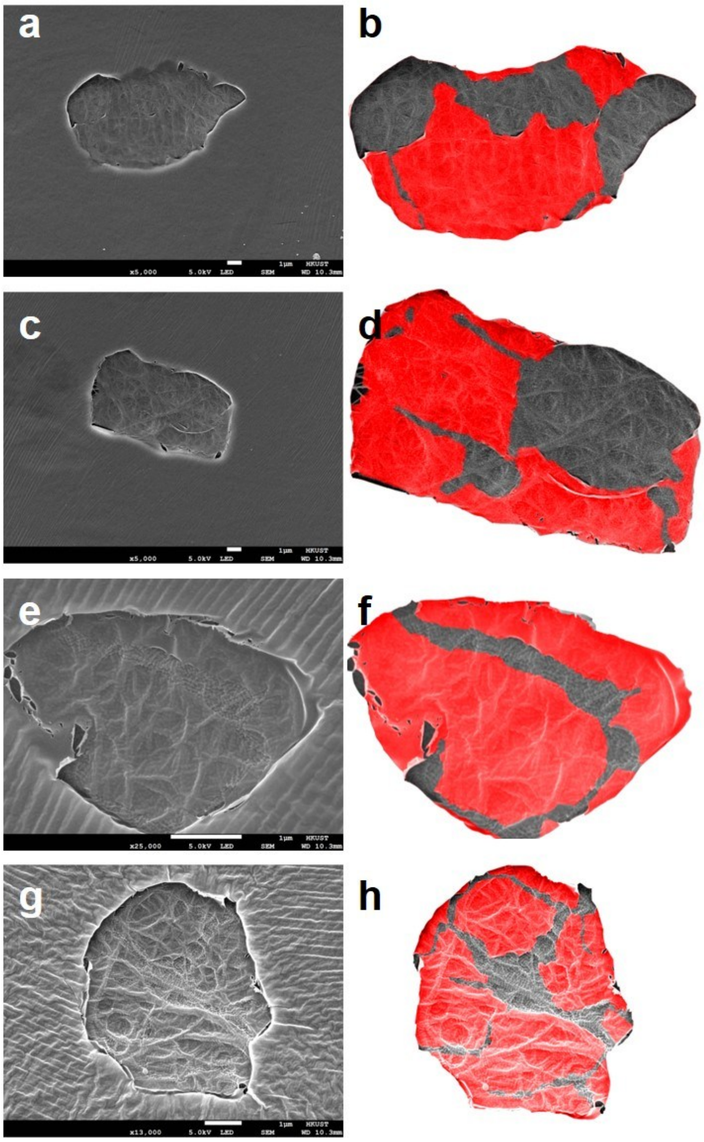

Fig. S7 Graphene transferred in pinholes of PE. (a, c, e, g) SEM micro-photograph of the pinholes on PE. (b, d, f, h) Graphene transferred in pinholes, as highlighted in red.

Graphene coverage in pinholes after exfoliation transfer was observed by SEM and the coverage was calculated as 53.69%, 59.09%, 84.12% and 79.60%, for (a), (c), (e) and (g) in **Fig. S7**, respectively.

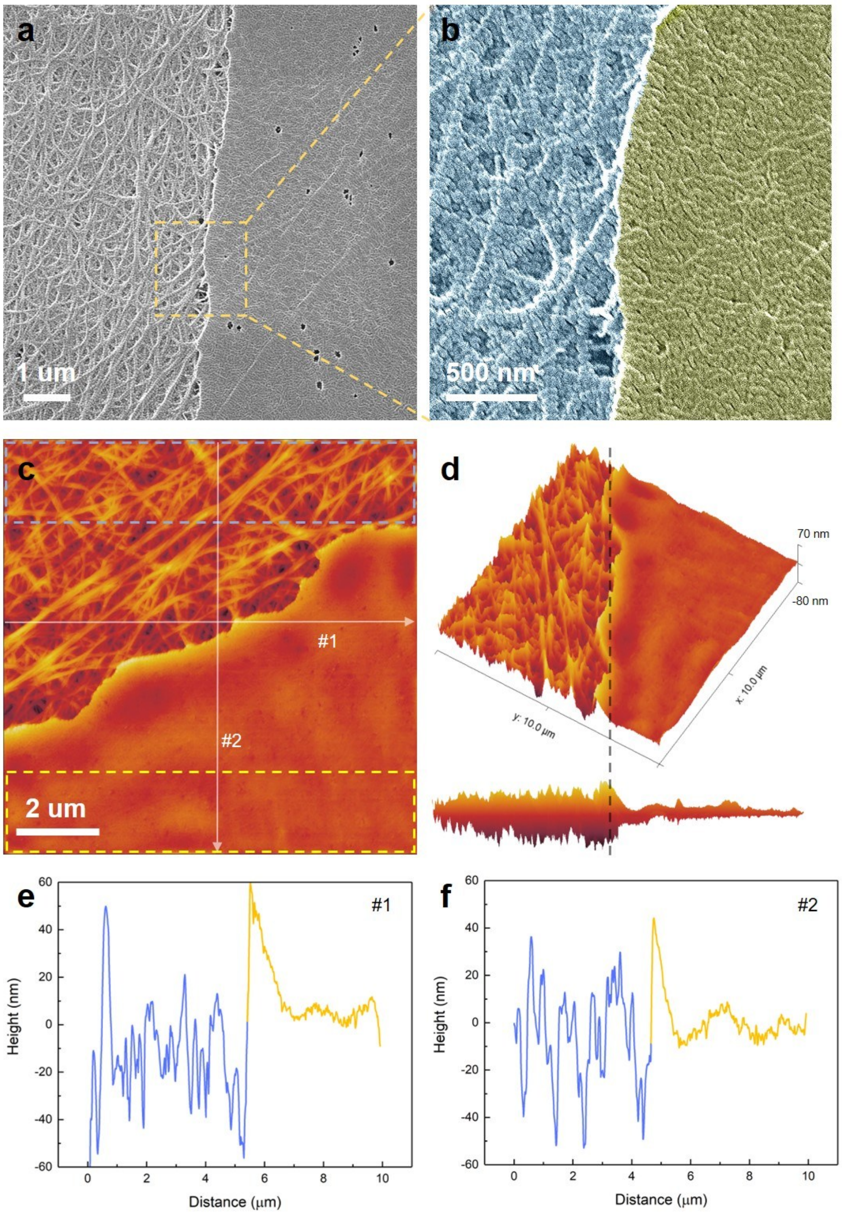

Fig. S8 Surface roughness of PE altered by annealing when attached to a copper foil only without graphene. (a) SEM microphotograph of surface morphologies of PE annealed at 140°C on a bare copper foil. The right-hand side was the PE area after exfoliating the copper foil, demonstrating a clear copper coverage boundary. The left-hand side PE went through annealing without any coverage, serving as a reference. (b) Magnified image of the lighted area of (a), focusing the copper coverage boundary. PE annealed attached to the copper foil was colored in yellow, and the reference PE in blue. (c) AFM height image of PE surface after annealing, with the upper part as the reference, and the lower part attached to the bare copper foil during annealing. The RMS roughness of light blue dash line enclosed area (20 μm^2, reference PE) was 19.2 nm, while that of yellow dash line enclosed area (20 μm^2, PE on copper foil) was 5.1 nm. (d) 3D view of (c), the overlapped black dash line indicates the copper coverage boundary before peeling off after annealing. Lower the insert demonstrates the “skyline” of the 3D height image, viewed along the copper coverage boundary. (e & f) Cross-sectional height profiles extracted along with white arrows #1 and #2 in (c), respectively. The profile segment of reference PE was colored with blue while that of PE on copper in yellow.

Graphene was excluded in this experiment to investigate the transfer mechanism of physical exfoliation. These results proved that the selective melting of PE and the substrate effect were two primary contributors to the transfer.

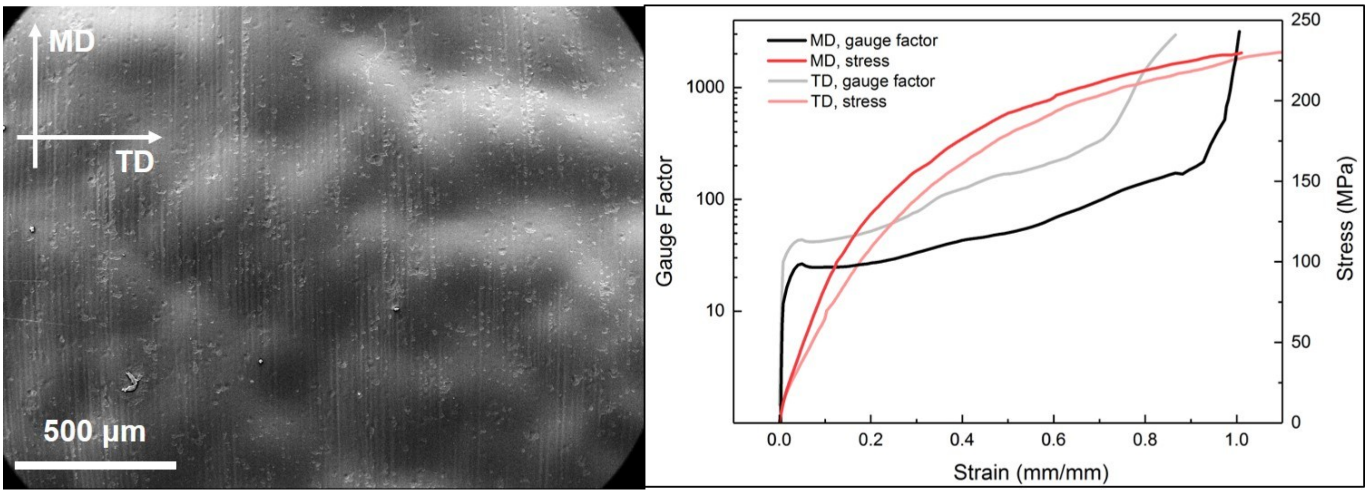

Fig. S9 Anisotropy of graphene and gPE piezoresistive sensor. (a) Low-magnification SEM micro-photograph of surface morphology of gPE. Machine direction (MD) parallels with CVD tube direction, and transverse direction (TD) is perpendicular to MD. (b) Gauge factor (logarithmic scale) and stress versus strain of gPE strain sensors during uniaxially tensile testing until fracture, in both MD and TD.

The graphene was CVD-grown in a quart tube, similar to the "roll-to-roll" method.[3] The steps along MD (along tube and gas flow direction during CVD) formed in the copper surface after CVD-growing substantially regulate the roughness and quality of graphene.[4] After direct physical exfoliation transfer, the defects or pinholes were principally distributed along MD, as shown in **Fig. S9a**. As demonstrated in **Fig. S8**, graphene could be transferred even in pinholes, but the coverage could not reach to 100%. Thus these aligned pinholes may serve as the crack initiator during stretching, especially along TD. As the cracks will develop faster in TD than MD, the conductive paths across graphene flakes will be diminished faster in TD. This discloses the anisotropy of gPE piezoresistive strain sensor in MD and TD as shown in **Fig. S9b**, although the underneath PE is isotropic in both crystallization (**Fig. S5**) and mechanical properties (strain and stress in **Fig. S9b**).

Table S1 Summary of typical piezoresistive strain sensors

Materials	Methods	Loading	Highest Gauge Factor
SWCNT wire/PDMS[5]	Embedding	2.0 wt%	10,000
MWCNT/TPU[6]	Twin-screw extruder	2.0 wt%	176
CBNP/elastomer[7]	Compression moulding	7.3 vol%	80
CNF yarn/TPU[8]	Embedding	1.0 wt%	1,700
Graphene woven fabrics/PDMS[9]	CVD/casting	N.A.	223
Glass fiber fabric/GO[10]	Dip coating	N.A.	480
Graphene woven fabrics/PDMS [11]	CVD/sandwich	N.A.	630
Graphene flakes/polymers[12]	self-assembly	4.4 nm in thickness	1037
Graphene/ecoflex[13]	encapsulation	N.A.	457

MWCNT: multi-walled carbon nanotubes;
TPU: thermoplastic polyurethane;
CBNP: carbon black nanoparticles;
CNF: carbon nanofibers;

References

1 X. Li, W. Cai, J. An, S. Kim, J. Nah, D. Yang, R. Piner, A. Velamakanni, I. Jung, E. Tutuc, S. K. Banerjee, L. Colombo and R. S. Ruoff, Large-area synthesis of high-quality and uniform graphene films on copper foils, *Science (New York, N.Y.)*, 2009, **324**, 1312–1314.

2 R. Li and P. Gao, Nanoporous UHMWPE Membrane Separators for Safer and High-Power-Density Rechargeable Batteries, *Global Challenges*, 2017, **1**, 1700020.

3 S. Bae, H. Kim, Y. Lee, X. Xu, J.-S. Park, Y. Zheng, J. Balakrishnan, T. Lei, H. Ri Kim, Y. I. Song, Y.-J. Kim, K. S. Kim, B. Özyilmaz, J.-H. Ahn, B. H. Hong and S. Iijima, Roll-to-roll production of 30-inch graphene films for transparent electrodes, *Nature Nanotechnology*, 2010, **5**, 574 EP -. DOI: 10.1038/nnano.2010.132.

4 G. D. Kwon, E. Moyen, Y. J. Lee, Y. W. Kim, S. H. Baik and D. Pribat, Influence of the copper substrate roughness on the electrical quality of graphene, *Materials Research Express*, 2017, **4**, 15604.

5 J. Zhou, X. Xu, H. Yu and G. Lubineau, Deformable and wearable carbon nanotube microwire-based sensors for ultrasensitive monitoring of strain, pressure and torsion, *Nanoscale*, 2017, **9**, 604–612.

6 J. F. Christ, N. Aliheidari, A. Ameli and P. Pötschke, 3D printed highly elastic strain sensors of multiwalled carbon nanotube/thermoplastic polyurethane nanocomposites, *Materials & Design*, 2017, **131**, 394–401.

7 C. Cochrane, V. Koncar, M. Lewandowski and C. Dufour, Design and development of a flexible strain sensor for textile structures based on a conductive polymer composite, *Sensors*, 2007, **7**, 473–492.

8 T. Yan, Z. Wang, Y.-Q. Wang and Z.-J. Pan, Carbon/graphene composite nanofiber yarns for highly sensitive strain sensors, *Materials & Design*, 2018, **143**, 214–223.

9 X. Liu, C. Tang, X. Du, S. Xiong, S. Xi, Y. Liu, X. Shen, Q. Zheng, Z. Wang and Y. Wu, A highly sensitive graphene woven fabric strain sensor for wearable wireless musical instruments, *Materials Horizons*, 2017, **4**, 477–486.

10 R. Moriche, A. Jiménez-Suárez, M. Sánchez, S. G. Prolongo and A. Ureña, Graphene nanoplatelets coated glass fibre fabrics as strain sensors, *Composites Science and Technology*, 2017, **146**, 59–64.

11 Y. Tang, Z. Zhao, H. Hu, Y. Liu, X. Wang, S. Zhou and J. Qiu, Highly stretchable and ultrasensitive strain sensor based on reduced graphene oxide microtubes–elastomer composite, *ACS applied materials & interfaces*, 2015, **7**, 27432–27439.

12 X. Li, T. Yang, Y. Yang, J. Zhu, L. Li, F. E. Alam, X. Li, K. Wang, H. Cheng, C.-T. Lin, Y. Fang and H. Zhu, Large-Area Ultrathin Graphene Films by Single-Step Marangoni Self-Assembly for Highly Sensitive Strain Sensing Application, *Adv. Funct. Mater.*, 2016, **26**, 1322–1329.

13 L.-Q. Tao, D.-Y. Wang, H. Tian, Z.-Y. Ju, Y. Liu, Y. Pang, Y.-Q. Chen, Y. Yang and T.-L. Ren, Self-adapted and tunable graphene strain sensors for detecting both subtle and large human motions, *Nanoscale*, 2017, **9**, 8266–8273.